IASF/CNR
SEZIONE BOLOGNA
LFI Project System Team

Planck LFI

TITLE: **Optimisation of the LFI Edge Taper values. I. FH #3 and #9 Main Beam and Full Pattern Simulations w/o Shields.**

DOC. TYPE: TECHNICAL NOTE
PROJECT REF.: PL-LFI-PST-TN-035 **PAGE:** I of IV, 14
ISSUE/REV.: 1.0 **DATE:** April 2003

Prepared by	M. SANDRI F. VILLA R. NESTI LFI Project System Team M. BERSANELLI LFI Instrument Scientist	Date: Signature:	April 16th, 2003
Agreed by	C. BUTLER LFI Program Manager	Date: Signature:	April 16th, 2003
Approved by	N. MANDOLESI LFI Principal Investigator	Date: Signature:	April 16th, 2003

DISTRIBUTION LIST

Recipient	Company / Institute	E-mail address	Sent
BERSANELLI M.	Univ. Di Milano – Milano	marco@mi.iasf.cnr.it	Yes
BUTLER C.	IASF-CNR Sez. di Bologna - Bologna	butler@bo.iasf.cnr.it	Yes
MANDOLESI, N.	IASF-CNR Sez. di Bologna – Bologna	reno@bo.iasf.cnr.it	Yes
MENNELLA, A.	IASF-CNR Sez. di Milano – Milano	daniele@mi.iasf.cnr.it	Yes
SANDRI M.	IASF-CNR Sez. di Bologna – Bologna	sandri@bo.iasf.cnr.it	Yes
VILLA F.	INAF – Arretri	villa@bo.iasf.cnr.it	Yes
NESTI R.	IASF-CNR Sez. di Bologna – Bologna		
BURIGANA C.	IASF-CNR Sez. di Bologna – Bologna	burigana@bo.iasf.cnr.it	Yes
LFI System PCC	IASF-CNR Sez. di Bologna – Bologna	lfispcc@tesre.bo.cnr.it	Yes

CHANGE RECORD

Issue	Date	Sheet	Description of Change	Release
1.0	16/04/03	All	First issue of document	==

TABLE OF CONTENTS

1 INTRODUCTION AND SCOPE 1

2 PARAMETERS OF THE PLANCK TELESCOPE 1

3 FOCAL PLANE UNIT CONFIGURATION AND FEED LOCATIONS 2

4 FEED MODELISATION 2

5 SIMULATION METHODS 5

5.1 MAIN BEAM SIMULATIONS 5
5.2 FULL PATTERN SIMULATIONS 5

6 MAIN BEAM RESPONSE 6

7 FULL PATTERN 9

8 REFERENCES 14

1 INTRODUCTION AND SCOPE

This technical note describes preliminary electromagnetic simulations performed on the LFI feed horns (FH) #3 and #9 coupled to the Planck telescope, with the aim of optimising the LFI Edge Taper (ET). The ET optimisation is mandatory to reach the LFI angular resolution requirement, and possibly the goal, preserving at the same time the needed straylight rejection. The analysis is carried out at 100 GHz, where the scientific benefit of gaining angular resolution is most important.

Five different FH designs have been considered: the FH #3 and #9 Qualification Model (QM) designs, and FH designs denoted with #3A, #9A, and #9B, which have been specifically designed with an edge taper that leads to an angular resolution of 12', 10', and 9.5', respectively, when Gaussian feed models are considered. For FH horn design the main beam and the full pattern have been computed. The effect of shields has not been considered here, and will be the subject of a forthcoming note.

2 PARAMETERS OF THE PLANCK TELESCOPE

The telescope parameters are slightly changed with respect to those presented in [1] according to the Telescope mechanical model [2] in order to have the rims of both the primary and secondary mirrors lying on a plane. Details of the coordinate systems defined to represent the telescope in GRASP8 and the telescope configuration are reported in [3]. In Figure 1 a sketch of the telescope and coordinate systems is shown.

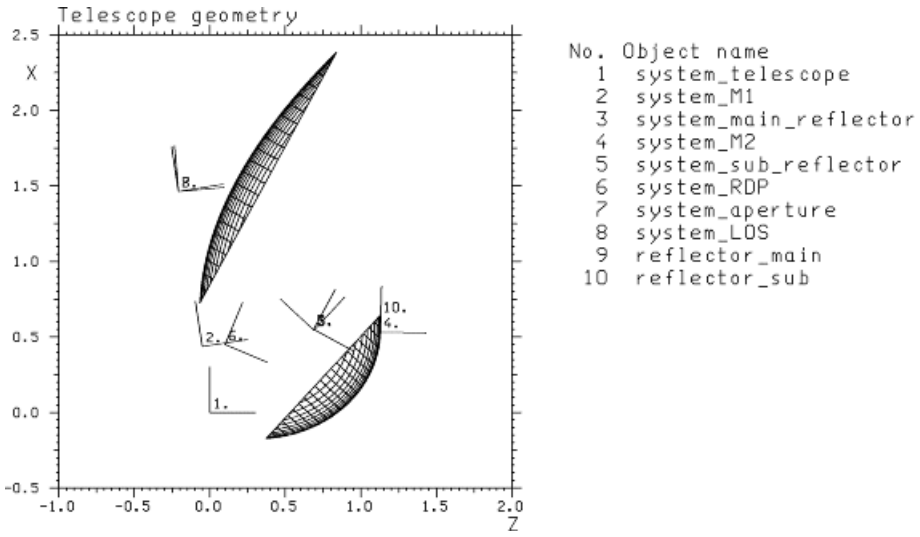

Figure 1 Coordinate systems defined for representing the telescope in GRASP8.

3 Focal Plane Unit configuration and Feed locations

For consistency with previous works, we consider here the layout of the LFI focal plane with the whole set of 27 corrugated feed horns located around the HFI FPU as reported in Figure 2[1]. In this study we concentrate on FH #3 and #9, marked with a red circle in Figure 2. The location of these feed horns defined in the Reference Detector Plane axis system (RDP), are $(X_{RDP},Y_{RDP},Z_{RDP})_{FH3}$ = (95.28, 42.80, -18.33) mm and $(X_{RDP},Y_{RDP},Z_{RDP})_{FH9}$ = (-40.95, 90.94, 7.48) mm. Their orientations are $(\theta_{RDP},\varphi_{RDP},\psi_{RDP})_{FH3}$ = (12.34, -157.14, -154.88) degrees and $(\theta_{RDP},\varphi_{RDP},\psi_{RDP})_{FH9}$ = (11.81, -66.93, -62.26) degrees.

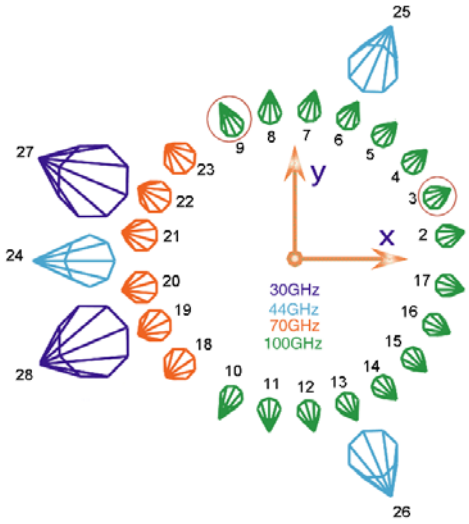

Figure 2 Planck/LFI Focal Plane Unit configuration.

4 FEED MODELISATION

Dual profiled feed horns have been used as a source in our electromagnetic simulations. In Table 1 the main FH characteristics are listed[2]. PG21 (LFI 3,16) and PG25 (LFI 9,10) represent the current Qualification Models. The Edge Taper of the other three horns has been chosen by means of optical simulations based on gaussian feed horns, in order to improve the resulting angular resolutions on the sky. For FH#3, when a certain edge taper degradation is reached, increasing the illumination on the primary mirror doesn't lead to any further improvement of angular resolution, because the strong illumination of the mirrors increases the aberrations on the main beam, as reported in [1]. For this reason, an angular resolution better than 12 arcmin is not achievable (PG28 – 3A). For FH #9, two different designs have been performed, PG27 (9A) and PG31 (9B), that lead to angular resolutions of 10 and 9.5 arcmin, respectively.

Far field pattern of each horn was computed by Modal Matching/MoM Models on a dual profile corrugated horn (by the CAISMI Institute, Florence – Italy) in 72 azimuthally equidistant cuts, in which θ ranges from 0° to 180. Figure 3 ÷ Figure 7 show the horn profile and the far field pattern for each 100 GHz dual profiled horn used in the simulations.

[1] The current baseline FPU layout foresees 23 horns in total, since the feeds #2,#3,#16, and #17 are not applicable anymore.
[2] RT: Return Loss, SLL: Side Lobe Level, PC: Phase Centre position from the aperture.

Table 1 Feed Horn characteristics.

Feed	ID	ν (GHz)	Δν/ν	Edge Taper	X-polar (dB)	RT (dB)	SLL (dB)	PC (mm)
LFI 3-16	PG21	100	20	28.3dB @ 24°	< -30	> 30	< -35	-12.21
LFI 3-16	PG28	100	20	19.0dB @ 24°	< -30	> 30	< -35	-12.21
LFI 9-10	PG25	100	20	25.5dB @ 24°	< -30	> 30	< -35	-1.27
LFI 9-10	PG27	100	20	19.0dB @ 24°	< -30	> 30	< -35	-1.27
LFI 9-10	PG31	100	20	15.0dB @ 24°	< -30	> 30	< -35	-1.27

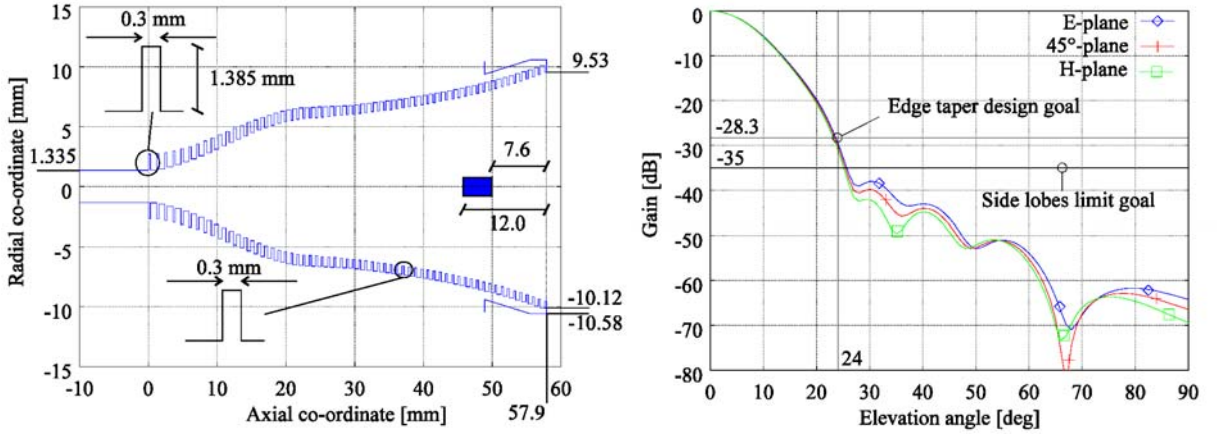

Figure 3 Feed Horn 3, 16 at 100 GHz - PG21. *Left:* Horn profile and (weighted) phase centre location. *Right:* Co-polar pattern

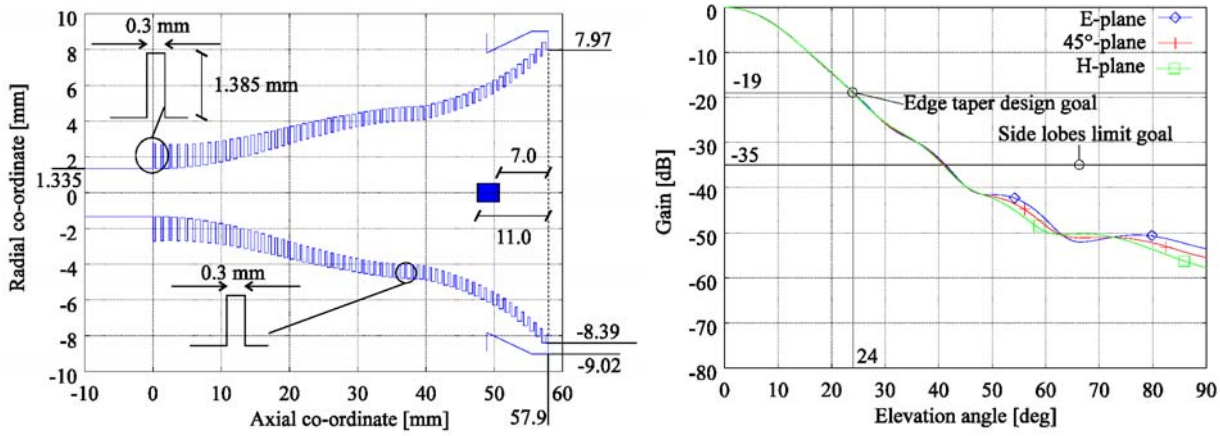

Figure 4 Feed Horn 3, 16 at 100 GHz - PG28. *Left:* Horn profile and (weighted) phase centre location. *Right:* Co-polar pattern

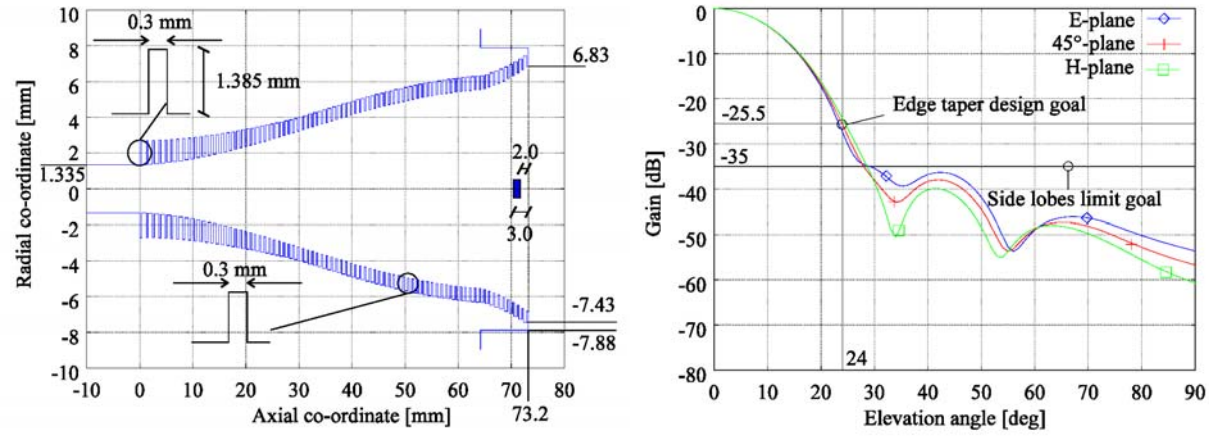

Figure 5 Feed Horn 9, 10 at 100 GHz - PG25. *Left:* Horn profile and (weighted) phase centre location. *Right:* Co-polar pattern

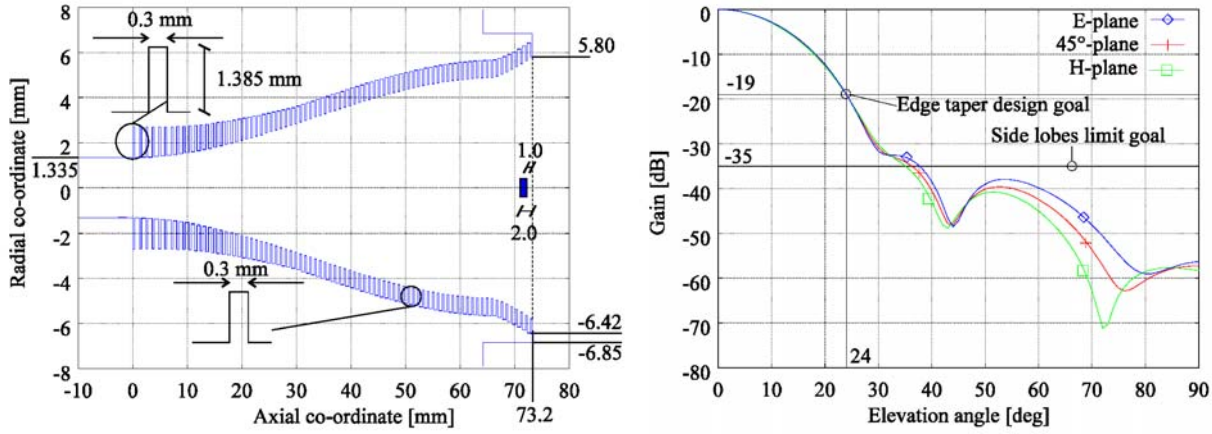

Figure 6 Feed Horn 9, 10 at 100 GHz – PG27. *Left:* Horn profile and (weighted) phase centre location. *Right:* Co-polar pattern

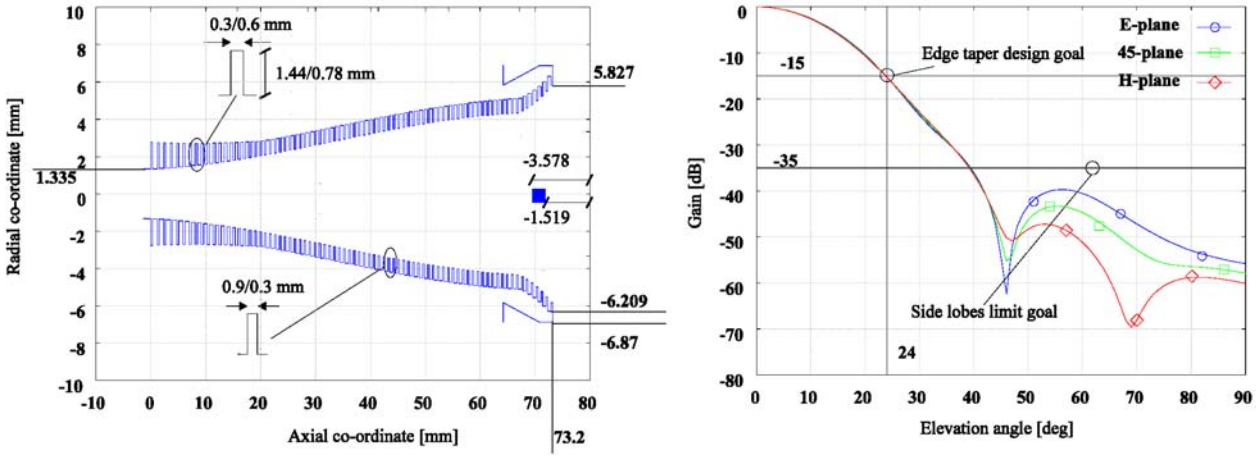

Figure 7 Feed Horn 9, 10 at 100 GHz – PG31. *Left:* Horn profile and (weighted) phase centre location. *Right:* Co-polar pattern

5 SIMULATION METHODS

The simulations have been performed considering the feed as a source and computing the pattern scattered by both reflectors on the far field. Different methodologies have been used for main beam and full pattern simulations.

5.1 Main Beam Simulations

- Main beams reported in Figure 8 ÷ Figure 12 have been computed in spherical UV grid (where $-0.015 \le U \le 0.015$,$-0.015 \le V \le 0.015$, with 301 x 301 points) using Geometrical Optics and Geometrical Theory of Diffraction (GO/GTD) on the sub reflector and Physical Optics (PO) on the main reflector [4].

- Main beams in spherical cuts (where $-5° \le \vartheta \le 5°$ and $0° \le \varphi < 180°$, $\Delta\vartheta = 0.5°$ and $\Delta\varphi = 0.5°$) have been computed using a full PO analysis (PO and PTD on each reflector).

5.2 Full Pattern Simulations

Full pattern simulations have been performed using Multi-reflector GTD (MrGTD), a new add-on package to GRASP8 developed by TICRA [5]. MrGTD is an advanced GTD method for evaluating the straylight rejection of the entire optical system. It computes GTD fields from any number of reflectors sequentially illuminated starting at a given source. It is a ray-optical frequency independent method that produces accurate results with a reasonable computation time (about one week for a full pattern computed without shields, on a single processor, 1 Gb RAM, CPU ALPHA21164, 533 MHz).
We specified the Planck telescope geometry, the source characteristics, the field points in which the radiation pattern has to be computed (spherical cuts in which $-180° \le \vartheta \le 180°$ and $0° \le \varphi < 180°$, $\Delta\vartheta = 0.5°$ and $\Delta\varphi = 0.5°$), and each contribution (reflections and/or diffractions) to be take into account to reach an accurate radiation pattern prediction.

The contributions considered in the simulations are:

1) feed ⇒ far field
2) feed ⇒ reflection on sub reflector ⇒ far field
3) feed ⇒ reflection on main reflector ⇒ far field
4) feed ⇒ diffraction on sub reflector ⇒ far field
5) feed ⇒ diffraction on main reflector ⇒ far field
6) feed ⇒ reflection on sub reflector ⇒ diffraction on main reflector ⇒ far field
7) feed ⇒ diffraction on sub reflector ⇒ reflection on main reflector ⇒ far field
8) feed ⇒ diffraction on sub reflector ⇒ diffraction on main reflector ⇒ far field
9) feed ⇒ diffraction on main reflector ⇒ diffraction on sub reflector ⇒ far field
10) feed ⇒ diffraction on main reflector ⇒ reflection on sub reflector ⇒ far field

6 MAIN BEAM RESPONSE

In this section we present the simulated main beams (co-polar and cross-polar components) of each feed horn under study. The contour plots normalized at peak gain are shown. X and Y (U and V) plotted range are [-0.015; 0.015]. Each beam is centred on the relative beam axis. The contour lines plotted are -3, -6, -10, -15, -20, -30, -40, -50, -60 dB. For each feed the angular resolution at different tapers is shown in Table 2, together with the principal characteristics of the main beam.

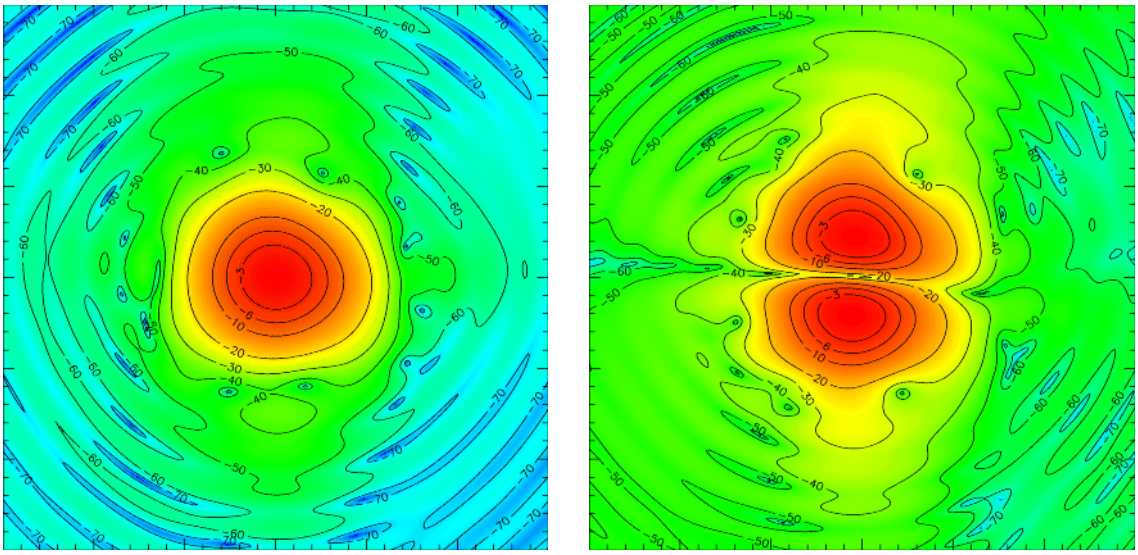

Figure 8 Main Beam 3 at 100 GHz – PG21. Co and Cross polar component.

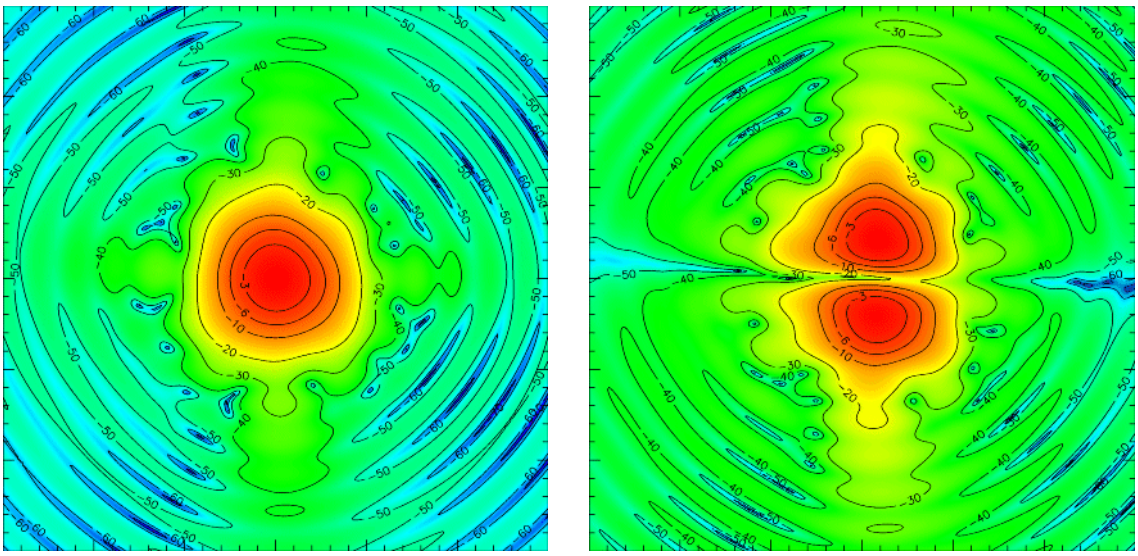

Figure 9 Main Beam 3 at 100 GHz – PG28. Co and Cross polar component.

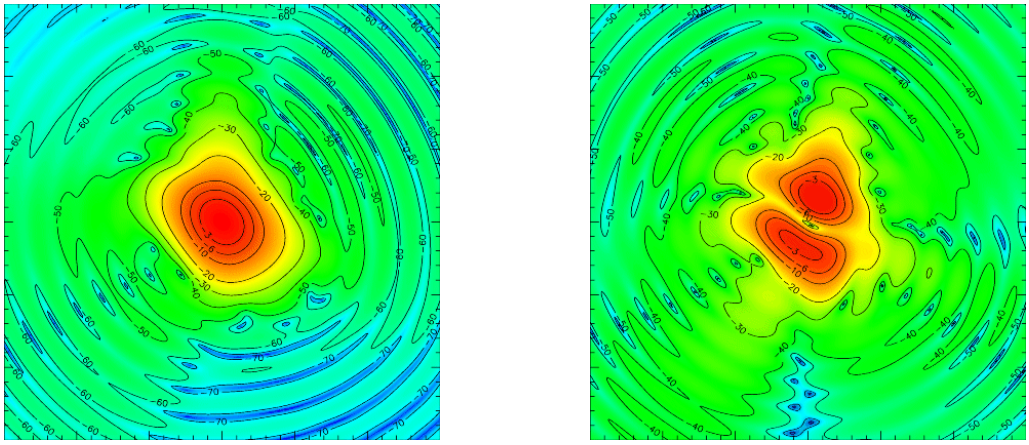

Figure 10 Main Beam 9 at 100 GHz – PG25. Co and Cross polar component.

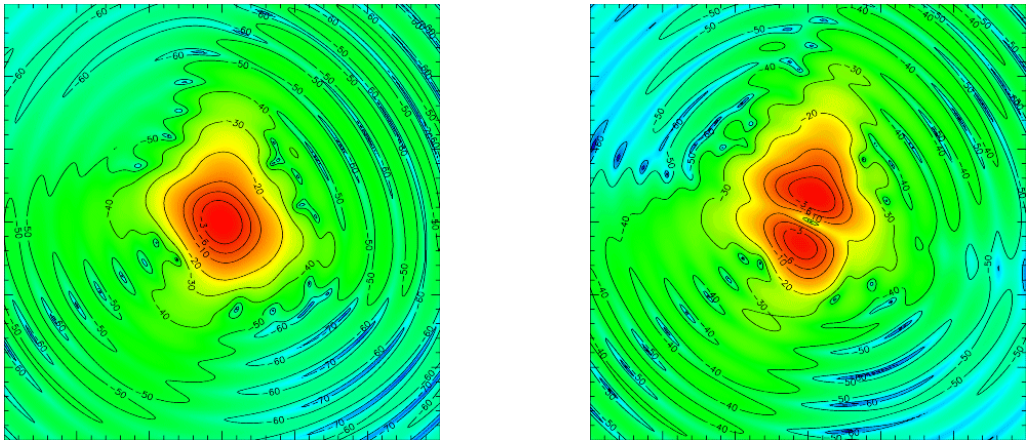

Figure 11 Main Beam 9 at 100 GHz – PG27. Co and Cross polar component.

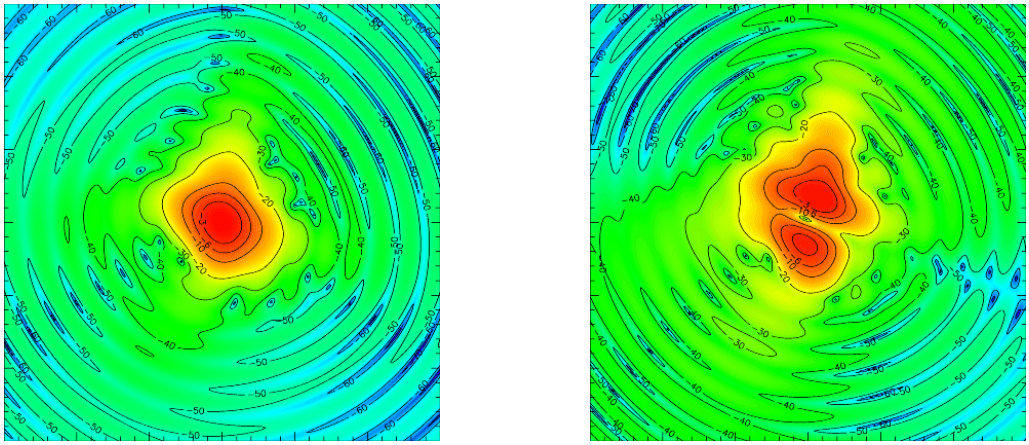

Figure 12 Main Beam 9 at 100 GHz – PG31. Co and Cross polar component.

Table 2 Main Beam characteristics.

Feed	ID	Co-polar max (dBi)	X-polar max (dBi)	Dir (dBi)	FWHM (arcmin)			PL (%)	PC (%)	D (%)	α (°)
					min	max	ave				
LFI 3	PG21	58.99	32.64	58.99	12.12	13.80	12.96	99.3613	0.0003	0.6387	-90.0
LFI 3	PG28	59.05	34.65	59.05	12.12	12.96	12.54	99.0256	0.0142	0.9744	-89.9
LFI 9	PG25	60.69	33.23	60.69	9.24	11.88	10.56	99.5508	0.0195	0.4492	89.8
LFI 9	PG27	61.13	33.90	61.13	8.88	11.16	10.02	99.4427	0.0071	0.5573	-89.9
LFI 9	PG31	61.19	35.10	61.19	8.52	10.56	9.54	99.3294	0.0478	0.6706	-89.7

Where:

- PL is the degree of linear polarization
- PC is the degree of circular polarization
- D is the degree of depolarisation
- α is the angle between the major axis of the polarization ellipse and the X_{MB} – axis

7 Full Pattern

In this section the full power pattern of each feed horn is shown. Figure 13 represents a sort of key for reading maps reported in Figure 15, Figure 16, Figure 18, Figure 19, and Figure 20. Each power pattern is shown from –60 to 60 dBi. The boresight direction is at the top of the map. The φ angle goes from 180° (left side of the map) to 0° (centre of the map), which corresponds to 180°. Then φ decreases from 180° to 0° again (right side of the map). Each polar cut with a constant φ value is a meridian of the map. The θ angle runs, on each meridian, from 0° (towards the main beam direction) to 180° (-180°) sweeping the map on its left (right) side. Therefore the centre of the map has φ and θ values equal to 0° and 90°, respectively. In Figure 13 the major contributions are pointed out. The Main Reflector Spillover is mainly due to reflection on sub reflector not intercepted by the primary mirror (Rs), diffraction on the main reflector (Dm), and diffraction on the sub reflector (Ds). The Sub Reflector Spillover is mainly due to the rays from feed which pass the secondary mirror (direct) and diffraction on the sub reflector (Ds). Another important contribution is caused by the feed side lobe (direct).

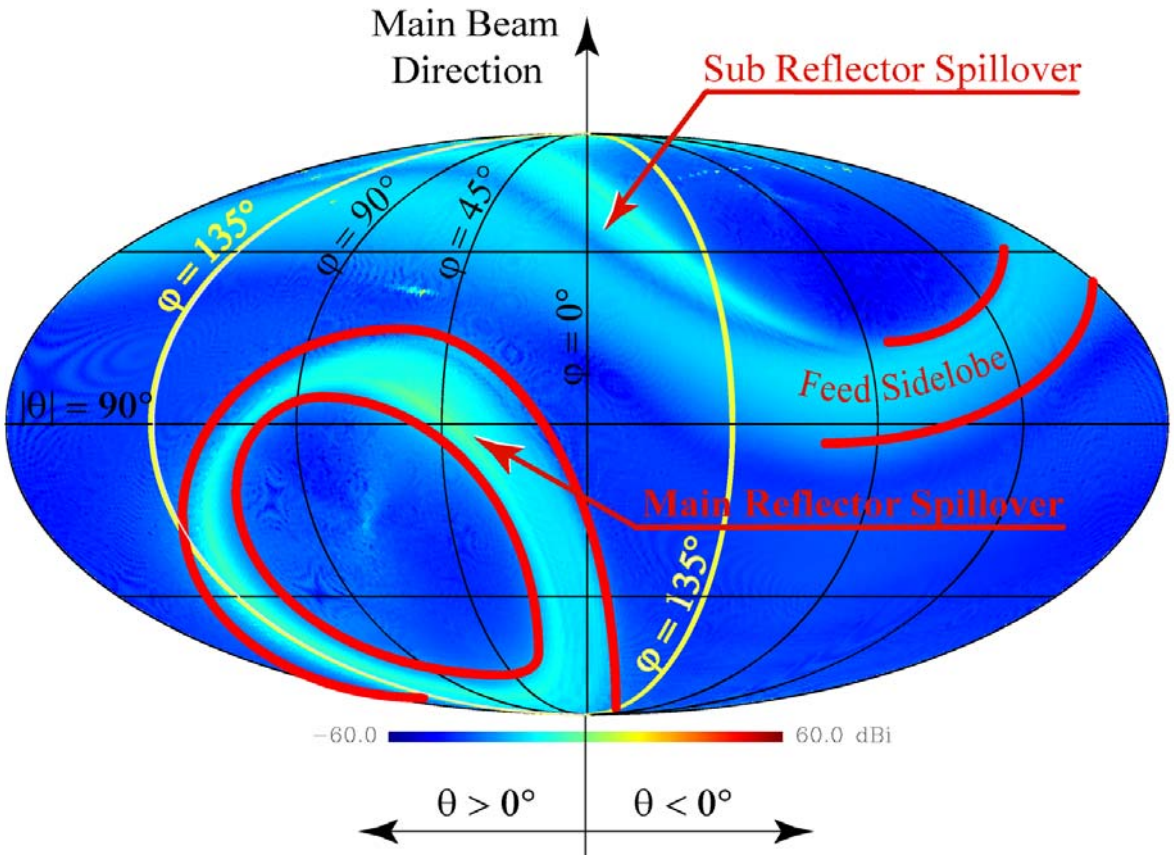

Figure 13 Example of a Full Pattern computed using GRASP8 MrGTD and plotted with HEALPix [6]. In the map, major contributions are pointed out, together with an indication of φ and θ angles (LFI9).

LFI3 @ 100GHz

The results are shown in Figure 14 for the cut at φ = 135°. It should be noted how the main spillover, at about φ = 135° and θ = 85° , raises increasing the illumination at the edge of the primary mirror (-15 dBi with an ET 28.3 at 24°, -4 dBi with an ET 19.0 at 24°) since it is due to diffraction and scattering from the edges of the mirror. At about θ = -75° sub spillover (-20 dBi with an ET 28.3 at 24°, -12 dBi with an ET 19.0 at 24°) can be recognized, and at about θ = -90° also the feed sidelobes. Cuts reported in Figure 14 can be seen in Figure 15 and in Figure 16 in a different representation and the peaks of the main reflector spillover can be easily identified.

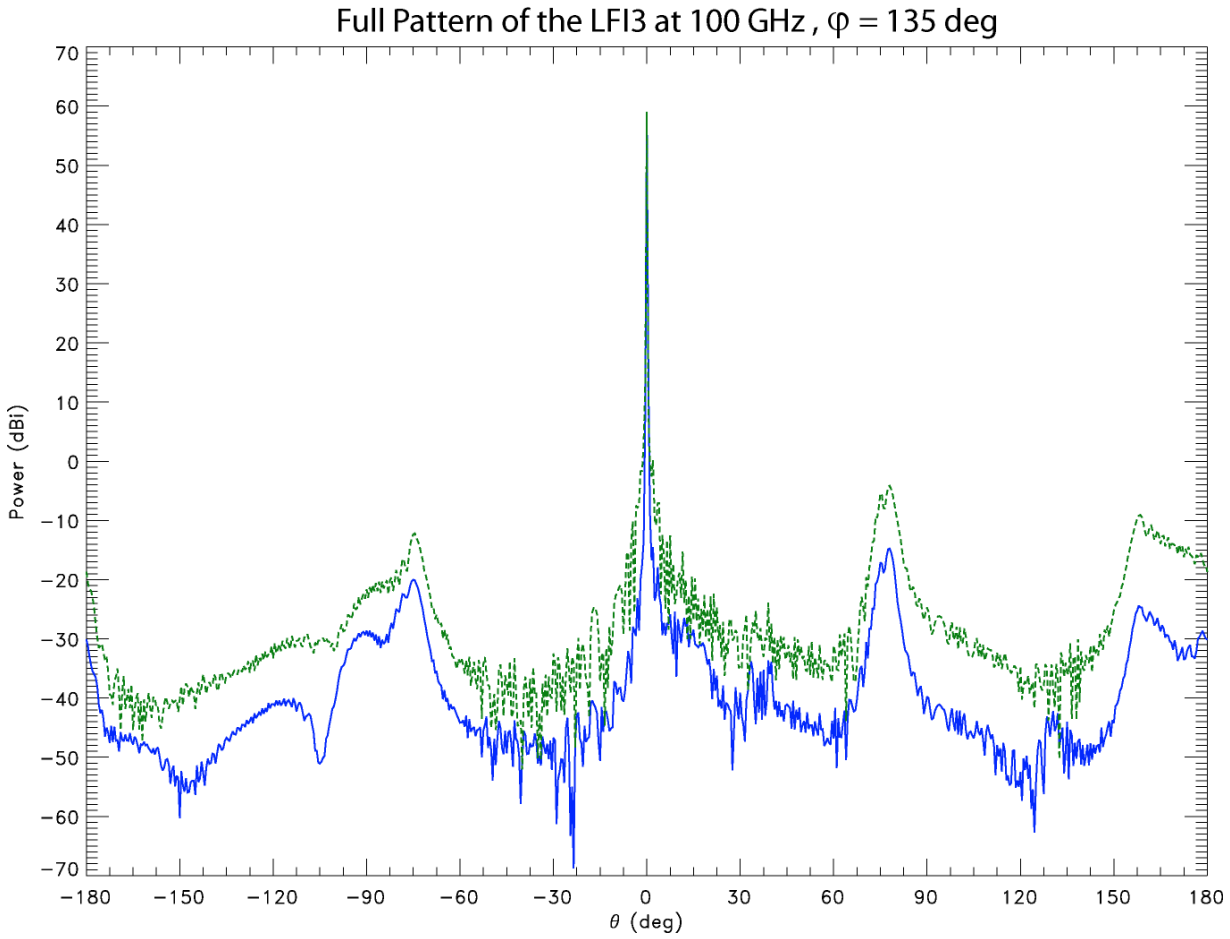

Figure 14 Full Pattern of the feed horn 3 at 100 GHz. Two curves with different ET are shown for the cut with φ = 135°: 28.3 dB at 24° (solid blue line), 19 dB at 24° (dashed green line).

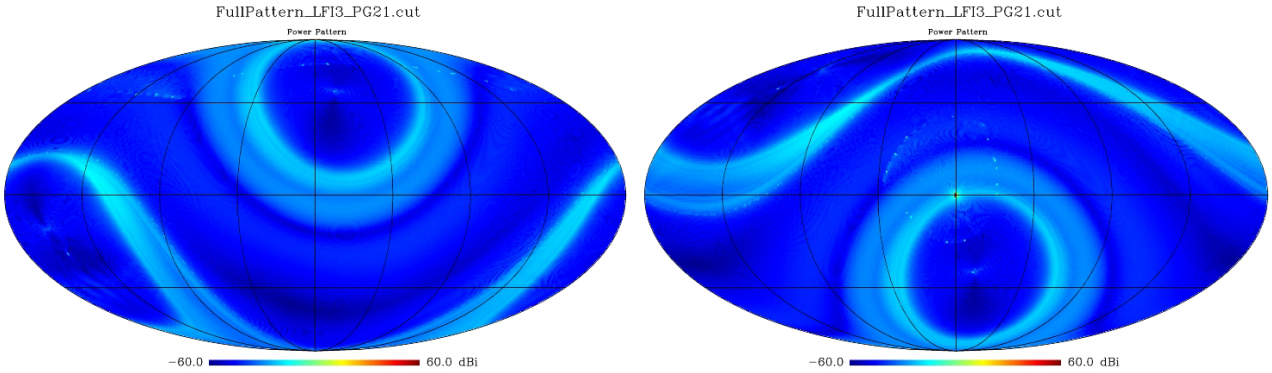

Figure 15 Full Pattern of the LFI3 – PG21 at 100 GHz (*power*). *Left:* the boresight direction is at the top of the map; *Right:* the boresight direction is in the centre of the map.

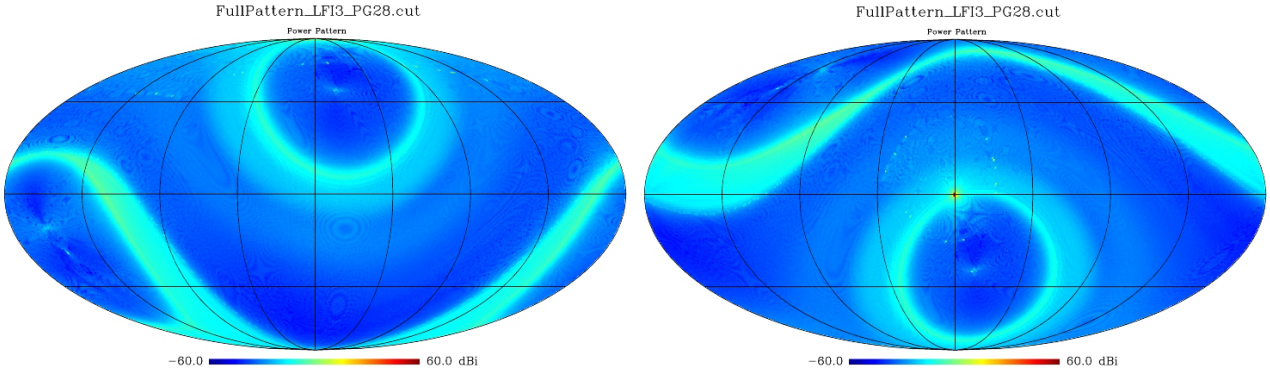

Figure 16 Full Pattern of the LFI3 – PG28 at 100 GHz (*power*). *Left:* the boresight direction is at the top of the map; *Right:* the boresight direction is in the centre of the map.

LFI9 @ 100GHz

The results are shown in Figure 17 for the cut at φ = 45°. It should be noted how the main spillover, at about φ = 45° and θ = 90° , raises increasing the illumination at the edge of the primary mirror (-7 dBi with an ET 25.5 at 24°, -2 dBi with an ET 19.0 at 24°, and 3 dBi with an ET 15.0 dB at 24°) since it is due to diffraction and scattering from the edges of the mirror. At about θ = -65° sub spillover (-25 dBi with an ET 25.5 at 24°, -20 dBi with an ET 19.0 at 24°, -26 dBi with an ET 15.0 at 24°) can be recognized. The lower level of the sub spillover for the feed with the higher edge taper is due to the different electromagnetic design of the horn, characterized by a lower sidelobe level (see Figure 7). In Figure 18 ÷ Figure 20 patterns over the full solid angle for the three LFI9 models considered are shown.

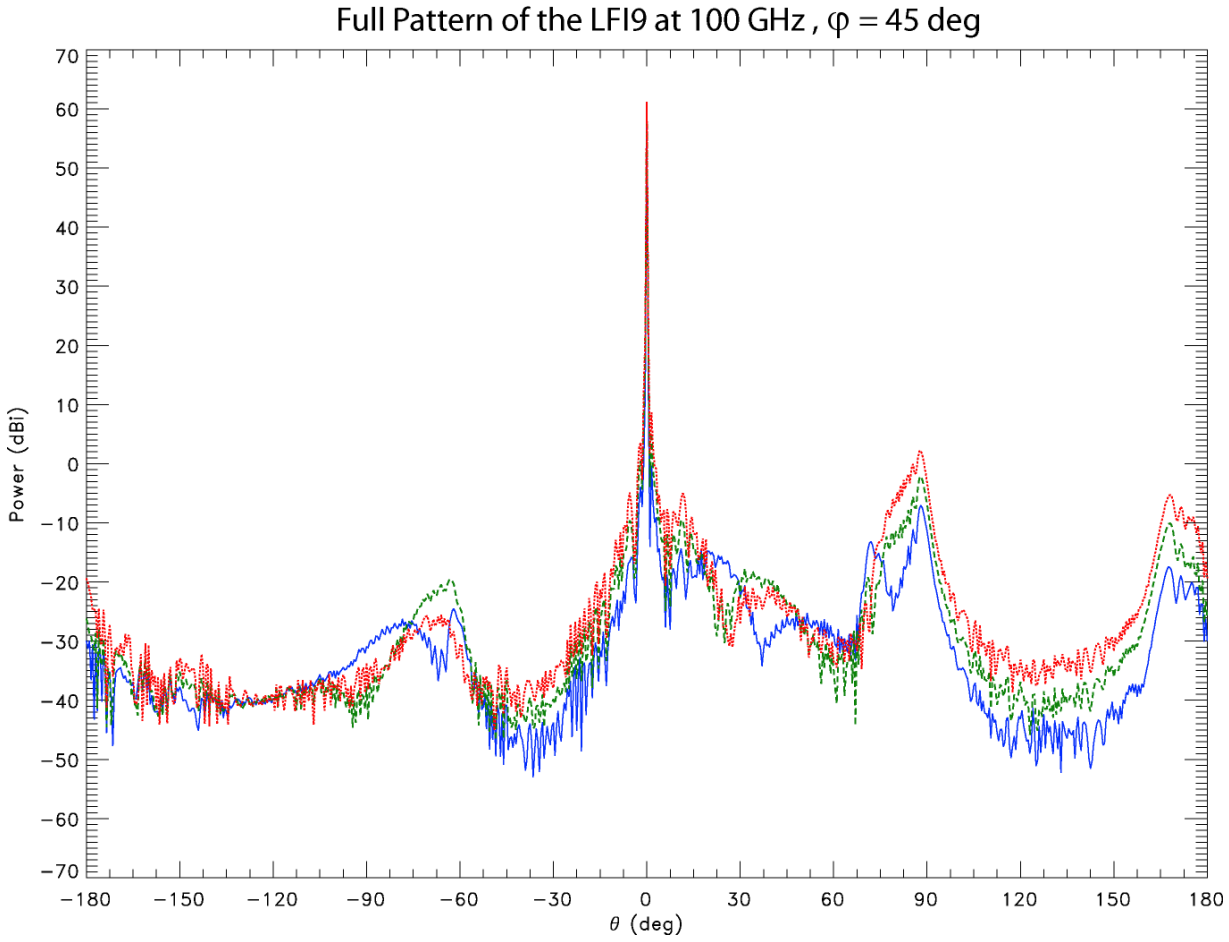

Figure 17 Full Pattern of the feed horn 9 at 100 GHz. Three curves with different ET are shown for the cut with φ = 45°: 25.5 dB at 24° (solid blue line), 19 dB at 24° (dashed green line), and 15 dB at 24° (dotted red line).

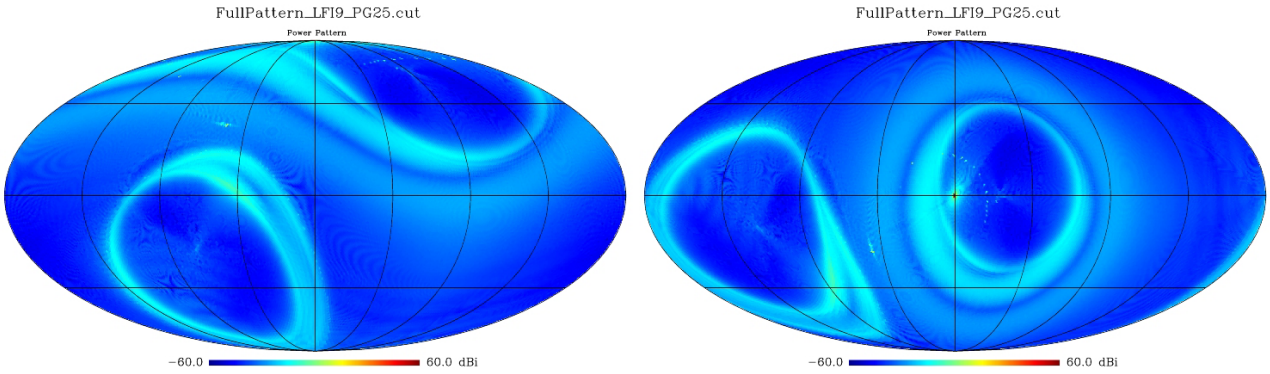

Figure 18 Full Pattern of the LFI9 – PG25 at 100 GHz (*power*). *Left:* the boresight direction is at the top of the map; *Right:* the boresight direction is in the centre of the map.

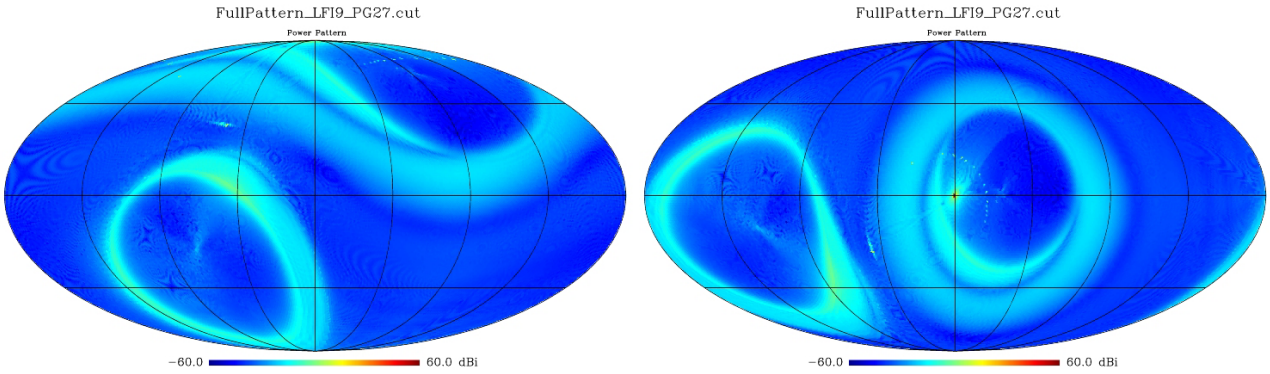

Figure 19 Full Pattern of the LFI9 – PG27 at 100 GHz (*power*). *Left:* the boresight direction is at the top of the map; *Right:* the boresight direction is in the centre of the map.

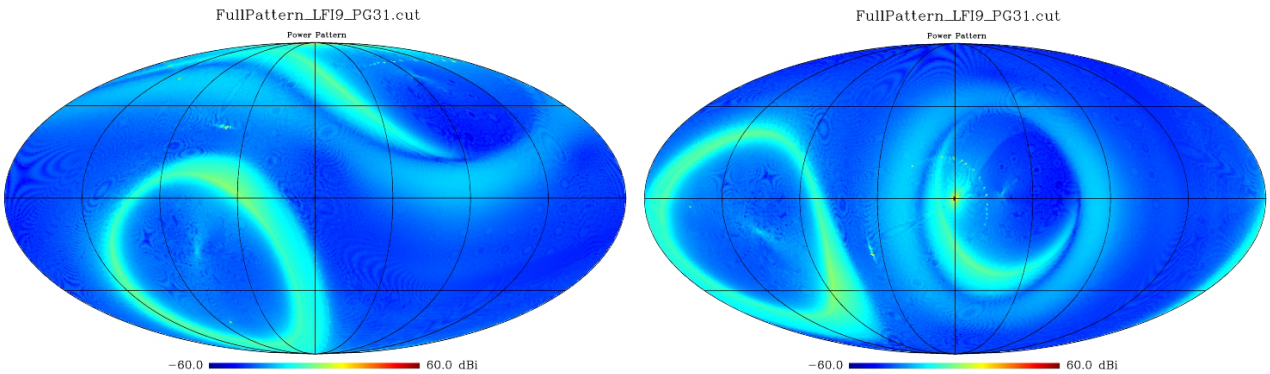

Figure 20 Full Pattern of the LFI9 – PG31 at 100 GHz (*power*). *Left:* the boresight direction is at the top of the map; *Right:* the boresight direction is in the centre of the map.

8 REFERENCES

1. M.Sandri, F.Villa, M.Bersanelli, N.Mandolesi, *PLANCK/LFI Optical Simulations: on the trade-off between angular resolution and edge taper*, Internal Report ITESRE 308/2001

2. *Planck PLM Design Report*, HP-3-ASPI-RP-0050

3. M.Sandri, F.Villa, *PLANCK/LFI Optical Simulations*: *a study on the full pattern prediction with GRASP8 Multi–Reflector,* Internal Report IASF Sezione di Bologna *in progress*

4. Knud Pontoppidan, 1999, *Technical Description of GRASP8*, TICRA. Doc.No.S-894-02

5. Per Nielsen, *Manual for Multi–reflector GTD: an add-on package to GRASP8*, TICRA. Doc.No.S-894-05.

6. K.M. Gorski, B.D. Wandelt, E. Hivon, F.K. Hansen, A.J. Banday, *The HEALPix Primer*, 1999.